

Received 31 October 2022; revised 12 November 2022; accepted 15 November 2022. Date of publication 24 November 2022;  
date of current version 3 February 2023. The review of this article was arranged by Associate Editor Xinge Yu.

Digital Object Identifier 10.1109/OJNANO.2022.3224462

# Design and Parametric Analysis of Charge Plasma Junctionless TFET for Biosensor Applications

D MANASWI<sup>1</sup>, SRINIVASA RAO KARUMURI<sup>1</sup> (Member, IEEE), AND GIRISH WADHWA<sup>2</sup>

<sup>1</sup>MEMS Research Center, Department of ECE, Koneru Lakshmaiah Educational Foundation (Deemed to be university), Guntur, Andhra Pradesh 522502, India

<sup>2</sup>Chitkara University Institute of Engineering and Technology, DICE Department Chitkara University, Punjab, India

CORRESPONDING AUTHOR: Srinivasa Rao Karumuri (e-mail: srinivasakarumuri@gmail.com)

**ABSTRACT** This paper presents a new design of charge plasma junctionless tunnel field effect transistor (CP JLTFET) with improved ON current, surface potentials. For the ease of fabrication, source and drain regions are induced in intrinsic silicon material using proper metal workfunctions. The rate of tunneling of electrons is found more in case of proposed CP JLTFET. The cavity length is varied between 8 nm and 10 nm and different dielectric constants have been used. This increased the ON state performance of device i.e ON drive current, potential and electric field. The increase in tunneling of electrons is mainly due to high recombination of carriers in the channel region. The proposed device simulated their electrical parameters like drain current, surface potentials, electric field, and energy bands with different dielectric constants. These excellent performance parameters of the proposed device with an appropriate material can be used for sensing application of biomolecules by introducing a cavity in the device.

**INDEX TERMS** Charge plasma, dielectric modulation tunnel FET, biosensor, biomolecule sensitivity.

## I. INTRODUCTION

In the current scenario, biosensors play a very important role in biomedical, medical engineering with the help of Nano-materials utilization. The development of biosensors targeted the applications in the field of medical, environmental and agricultural [1], [2], [3], [4]. A biosensor device is used to determine the existence of biological molecules, for example proteins, nucleotides etc. [5], [6]. To detect the biomolecules, Biosensor devices are developed based on FETs due to its advantages such as easy design, low cost etc. In recent decades, good number of biosensors design based on FET like Ion sensitive field effect transistor (ISFET), dielectric modulated field effect transistor (DM-FET), Si-Nanowire Tunnel Field effect Transistors [7], [8], [9], [10]. All these devices are experiences a issues like short channel effects (SCEs), ultra doping profile. By increasing the gate terminals one can reduce the issue of SCE's but in nanoscale devices, doping profile is still a major problem in the fabrication process. There is one solution to overcome this problem is junctionless field effect transistor [11], [12], [13].

From Literature, number of researchers have been presented the designed and the fabrication aspects of the junctionless field effect transistor. This device is easy to fabricate because throughout the substrate the doping profile is same and it has good improvements in electrical parameters as compare to MOSFETs. The subthreshold swing (SS) is one of the important parameter in TFET, here this parameter is better for JLTFET. Junctionless tunnel field effect transistor overcomes the issues of SS and fabrication process [14], [15], [16], [17], [18], [19].

The JLTFET has been design with gate underlap region, here both sides of gate materials etched along with dioxide layer to introduce the region of cavity which is useful for binding the biological molecules [20], [21], [22]. Biosensors based on JLTFET shows good improvements in electrical parameters such as drain current, energy bands, surface potential, electric field, threshold voltage of gate underlap in comparison with conventional DM-TFET [10], [23], [24], [25], [26]. Here, we have proposed a biological sensor based on double gate dielectric modulated JLTFET for the purpose of detection of

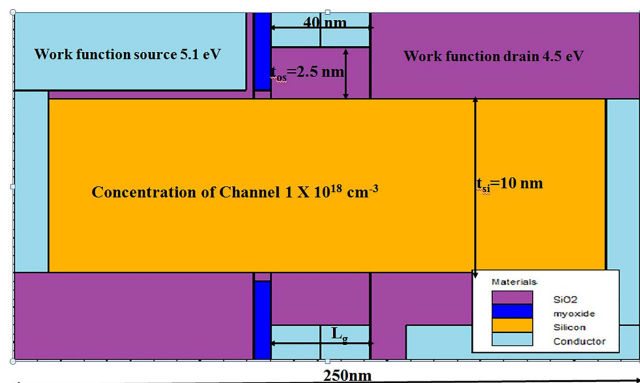


FIGURE 1. The schematic view of the proposed TFET device.

biological molecules both neutral and charged. A nanocavity region is created to permit the immobilization of biological molecules on the tunneling junction within the device. The wet etching process is preferred to make a nanocavity in the proposed device. We have observed the electrical parameters drain current, energy bands, electric field, surface potential of the proposed device. So consider this into account, the DG DMJLTTFET device is simulated for different dielectric materials with various biological molecules based on its dielectric constants.

In this paper, we have find out the performance parameter i.e sensitivity of the proposed device when the nanocavity filled with both the charge molecules. Also, different values of relative permittivity of biomolecules effects on drain current, energy bands, electric field, and surface potential for neutral and charged biological molecules is explored. The paper organizes as follows, In Section II, we have discussed the proposed device structure and its specifications. In Section III, we have discussed the characteristics of the proposed device in the presence of both the charged molecules followed by conclusions in Section IV.

## II. THE PROPOSED DEVICE & ITS DIMENSIONS

The schematic view of the proposed device as shown in Fig. 1. The Proposed device of the channel is divided into two regions. The proposed device of its cavity length taken as 8 and 10 nm and the oxide layer ( $\text{HfO}_2$ ) whose length is taken as 42 and 40 nm. The metal work function of both the gates is 4.5 eV. The spacer between the gate and source ( $L_{gs}$ ) is 3 nm and between gate and drain ( $L_{gd}$ ) is 15 nm [27], [28], [29].

The schematic view of the proposed device structure and its calibrated drain current characteristics curve shown in Fig. 1. We have considered an appropriate metal work function of electrodes on ultrathin silicon film with induced regions of source and drain (S/D) in the proposed device. The “p+” type source is framed in the intrinsic silicon substrate by using metal electrode (work function=5.1eV) which creates majority of positive charge carries i.e holes in the source side. In the similar way the “n+” type drain is framed in the intrinsic silicon substrate by (work function= 4.5eV) which creates

**TABLE 1.** The Proposed Device Dimensions and Its Parameters Used in Simulation

Parameters	Dimensions
Device Length	250 nm
Length of the gate overlap area ( $L_g$ )	42 nm and 40 nm
Length of the nanocavity region ( $L_{\text{cavity}}$ )	8 nm and 10 nm
Gate Work -functions	3.91 eV and 4.2 eV
Width of the Cavity region	2.5 nm
Length of the Spacer ( $L_{gs}$ )	3 nm
Oxide thickness	2.5 nm
Silicon thickness	10 nm
Concentration of Channel	$1 \times 10^{18} \text{ cm}^{-3}$

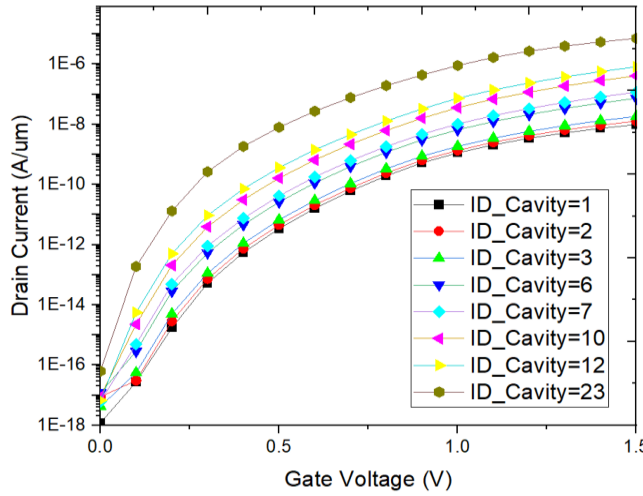
majority of negative charge carries i.e electrons in the drain side.

Table 1, provides the parameters of the proposed device used in simulation. All simulation parameters are taken constant for all the three architectures. For proper functioning, the thickness of intrinsic silicon substrate kept within the Debye length  $((\epsilon_{Si} * V_T)/q + 60 * N)^{1/2}$ , where  $n$ ,  $\epsilon_{Si}$ ,  $V_T$ , and  $q$  are substrate carrier concentration, silicon dielectric constant, thermal voltage and electronic charge of the silicon respectively [30], [31], [32], [33], [34]. To minimize the quantum mechanical effects, a 10 nm thickness silicon body is considered. A  $\text{SiO}_2$  layer of thickness 0.5 nm and 3 nm is placed between metal electrodes of source and drain respectively. A 3 nm and 15 nm spacer thickness are used between source-gate and drain-gate respectively. The parameters utilized in simulation for conventional JLTTFET [35], [36] are: highly doped carrier concentration  $n_i = 1.0 \times 10^{19}/\text{cm}^3$ , silicon film thickness = 10 nm, gate silicon dioxide thickness ( $t_{ox}$ ) = 2.5 nm, channel length ( $L$ ) = 7 nm and gate work function = 4.3 eV. For inducing holes having equivalent concentration of  $1 \times 10^{18} / \text{cm}^{-3}$  in the source region, platinum metal electrode is utilized.

All the simulations are carried out in ATLAS Silvaco TCAD simulator [37], [38], [39], [40] to understand and compare the physical process of architectures. The Non-local BTBT model is employed to find the recombination tunneling generation rate. To study the reverse and forward tunneling, quantum tunneling region is placed at the junctions of drain-channel and source-channel. To account for carrier recombination, Shockley-Read-Hall and Auger recombination models are invoked.

## III. RESULTS AND DISCUSSIONS

The dielectric constant represents the kind of biomolecules. There are two types of biomolecules i.e neutral and charged. The neutral biomolecules of their simulations based on dielectric constants while the simulation of charged biomolecules based on the dielectric constants as well as the charge density. The biomolecules of their immobilization induces band to band tunneling process for different dielectric constants and interfacing charges from source to channel region. There



**FIGURE 2.** Transfer characteristics of the proposed device with cavity region length = 8 nm.

are variations in drain current as the cavity region length varies due to the immobilization of biomolecules. From Fig. 2, it clear that the variety of biomolecules in the cavity have different kind of dielectric constants and with cavity region length 8 nm at  $V_{ds} = 1V$ .

The cavity region consists of air is represented by the notation ‘ID\_Cavity = 1’. Similarly, cavity region is filled with biomolecules of dielectric constant 2 is represented by ‘ID\_Cavity = 2’ and so on. The cavity regions are introduced in the proposed device under the gate, the tunneling barrier width increases due to low electron tunneling arises. After introducing the biomolecules in the cavity region of the proposed device, the tunneling barrier width decreases with the increment in dielectric values as shown in Fig. 2. The OFF current at drain is remains constant because there is increase in the energy band curve which leads to the depletion of the tunneling barrier width. The reduction of the tunneling barrier width does more curving the energy band that will leads to more tunneling of electrons between the conduction and valance band of the source.

For different dielectric values of the proposed device with cavity region of 10 nm at  $V_{ds} = 1.0V$ , the drain current variations due to the immobilization of number of biomolecules as shown in Fig. 3. It is observed from Fig. 3, there is changes in the drain current when the cavity region length increases from 8 nm to 10 nm. This slightly change in drain current is occurs due to the tunneling principle. Also observed that increase in cavity region length that impact on the tunneling barrier width widens which in turns leads reduce the tunneling probability. The reason behind is when we increase the cavity region length, that reduces the capacitance between the channel and the gate. Hence, the cavity region length increase in the proposed device impact the drain current i.e decreases.

The charged biomolecules are considered both dielectric values and interfacing the charges (ID\_Nf). When the positive charged biomolecules are immobilized in the proposed

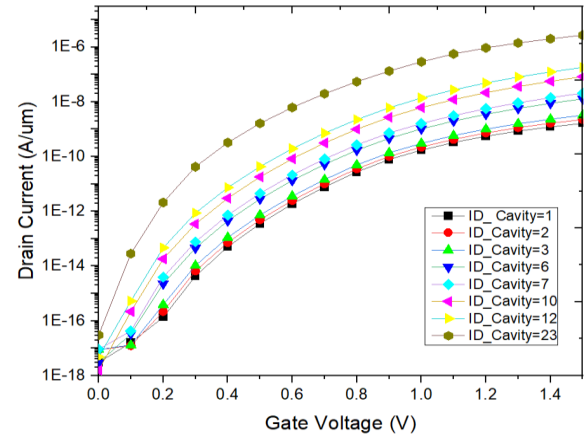
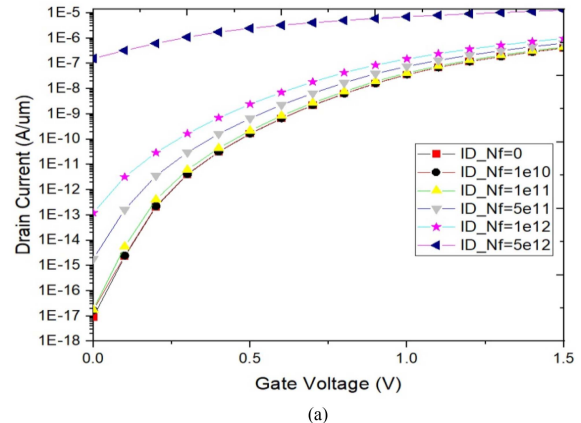
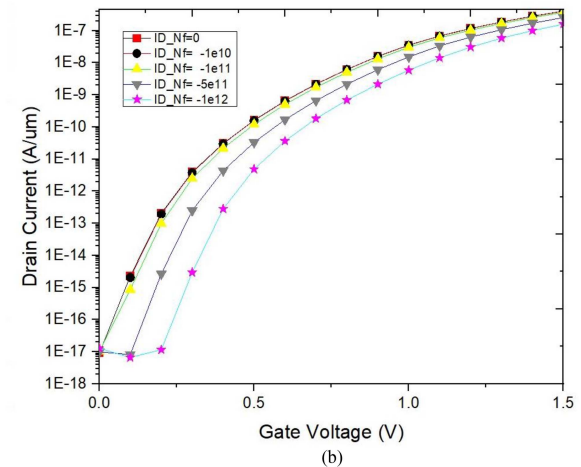


**FIGURE 3.** Transfer characteristics of DLDGTFT with different value of cavity for cavity length = 10 nm.



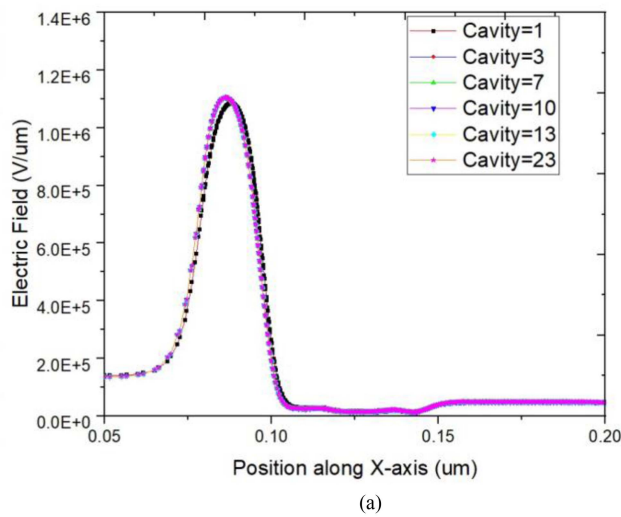
(a)



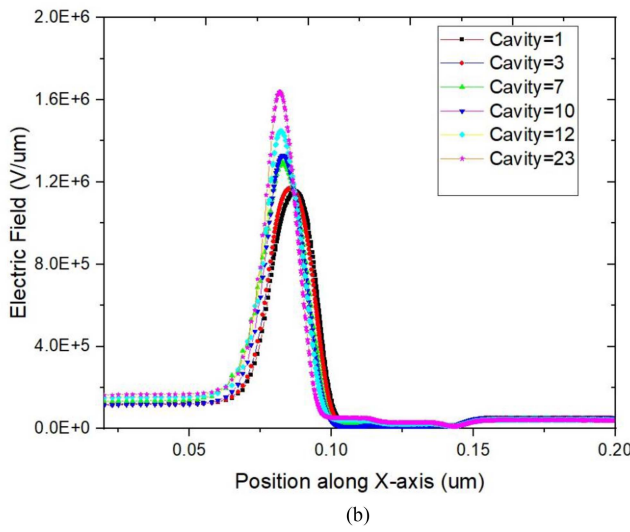
(b)

**FIGURE 4.** Drain current for DLDGTFT with cavity length = 8 nm for different (a) Positive interfacing charges and (b) Negative interfacing charges.

device under gate, there is variation in drain current shown in Fig. 4(a). It is known that the charge is proportional to the current, therefore an increase in the interfacing charges, the drain current increases because it decreases the tunneling barrier width. When negative charged biomolecules are immobilized in the proposed device under the gate as shown in



(a)

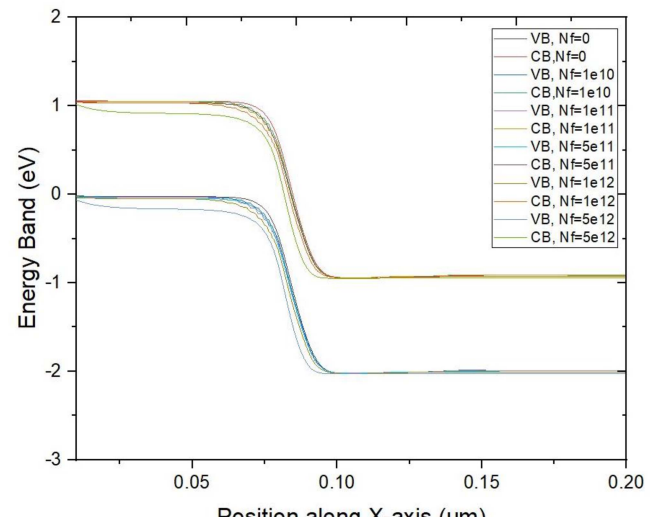


(b)

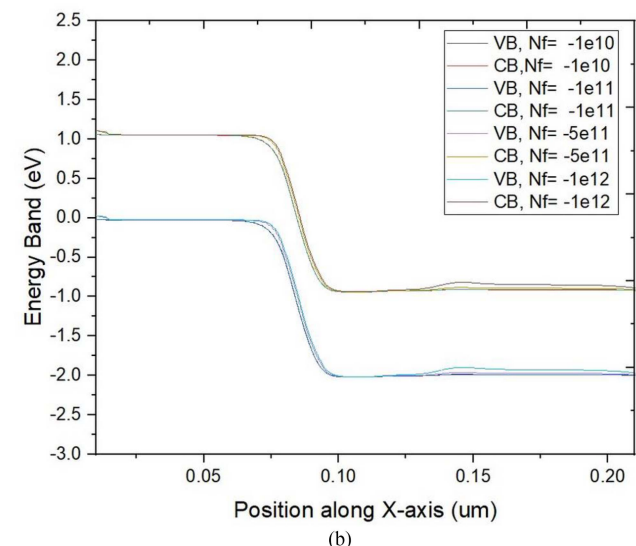
**FIGURE 5.** Effective electric field with different cavity at (a) Cavity length = 8 nm and (b) Cavity length = 10 nm.

Fig. 4(b). For negative charged biomolecules the drain current is low comparatively due to low charge density. The drain current for the negative charged biomolecules increases with increase in the interfacing charges and the OFF state current is remains constant. The variation in drain current is same as for positive charged biomolecules i.e the drain current increases with respect to increase in the charge density.

The variations in the electric field for different dielectric values of biomolecules as shown in Fig. 5. It is observed that the electric field is higher for the higher dielectric values of biomolecules. This is happened when gate voltage is applied for the proposed device, it induces the electric field. We know that the length of the cavity region is highly influence by the electric field, from Fig. 5(a), (b), it is observed that the higher dielectric constant produces higher electric field in the proposed device and the more electric field produces more tunneling of electrons which in turns produces high drain current.



(a)



(b)

**FIGURE 6.** Energy band diagram with cavity region of 8 nm for K = 10 for (a) Different positive interfacing charges. (b) Different negative interfacing charges.

Fig. 6(a) holds the same explanation for the increased cavity length i.e., 10 nm as it was for the charged biomolecules for cavity length 8 nm. It is observed that an increase in the positive interfacing charges will increase the drain current. This happens due to lowering of the tunneling barrier between the conduction and the valence band as shown in Fig. 6(b).

Fig. 6(a) shows an increase in the drain current because the charge density of the negatively charged biomolecules increases due to the same fact that the tunneling barrier reduces and the tunneling probability of the electrons increases which leads to a higher drain current as seen in Fig. 6(b). In spite of all, the OFF state current remains constant throughout.

For measuring the performance of the proposed device as a biosensor, the drain current sensitivity is one of the main factor we have considered in our investigation. The proposed device of its drain current sensitivity characteristics

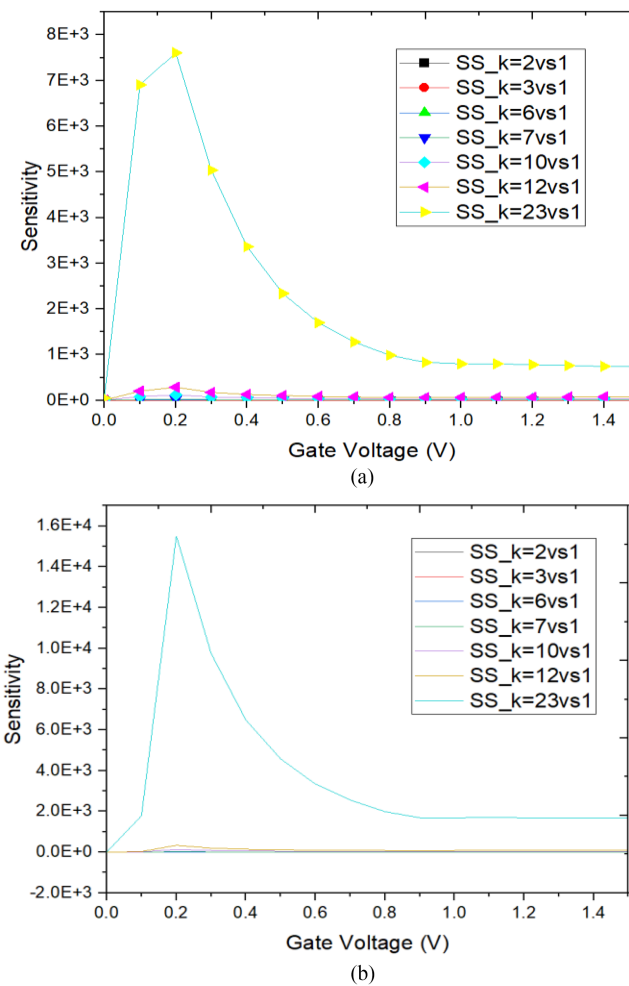


**FIGURE 7.** The sensitivity of the proposed device of cavity length (a)  $L_g = 8\text{ nm}$  (b)  $L_g = 10\text{ nm}$ .

with nanocavity region length 8 nm and 10 nm respectively at  $V_{DS} = 1.0\text{V}$  are shown in Fig. 7(a) and (b). The sensitivity factor of the proposed device when biomolecules with dielectric value 3 is taken into account with respect to air is noted as 'SS<sub>k</sub> = 2vs1 and so on. As we have seen that drain current is associated with dielectric values. Here, from Fig. 7(a) and (b), we have observed that the sensitivity of the proposed device is increases with the drain current of cavity length 8 nm and 10 nm. The sensitivity has been improved when the nanocavity region length is 8 nm and also whenever there is moderate change in the dielectric values. Therefore, the proposed device have ability to sense the biomolecules because it is directly proportional to the drain current sensitivity.

#### IV. CONCLUSION

In this paper, we have design and simulated the proposed DGDM JLTFTET device with nanocavity of 8 nm and 10 nm for different dielectric constants. As we know that TFET is like p-i-n transistor and the fabrication of the device is very complex as it has abrupt junctions but the proposed JLTFTET overcome the issue of abrupt junctions. We have simulated

and analyzed the proposed with different dielectric values like  $K = 1$  to  $K = 23$  for the detection of biological molecules. The proposed device induces the source and drain region with suitable workfunctions in the intrinsic channel area. In our analysis, the proposed device have shown pronounced electrical parameters like drain current, surface potential for various nanocavity regions. We have observed that the charge carriers recombination rate increases for the proposed device and this impact and improvements in drain current, surface potential, electric field and energy bands. By introducing the nanocavity with length of 8 nm for the proposed device under gate overlap region, the improvement in performance parameters, that shows the proposed device is more suitable for biosensing applications. In our future work, we will analyze the sensitivity of the proposed device as biosensor.

#### REFERENCES

- [1] P. Bergveld, "The development and application of FET-based biosensors," *Biosensors*, vol. 2, no. 1, pp. 15–33, 1986.
- [2] S. Anand, S. I. Amin, and R. K. Sarin, "Performance analysis of different material based dual electrode doping-less TFET," *Eur. Adv. Mater. Congr.*, vol. 2, no. 6, pp. 384–387, Apr. 2017.
- [3] G. Leung and C. O. Chui, "Variability impact of random dopant fluctuation on nanoscale junctionless FinFETs," *IEEE Electron. Device Lett.*, vol. 33, no. 6, pp. 767–769, Jun. 2012.
- [4] M. J. Kumar, R. Vishnoi, and P. Pandey, *Tunnel Field-Effect Transistors (TFET): Modelling and Simulations*. Hoboken, NJ, USA: Wiley, 2017.
- [5] P. H. Woerlee et al., "RF-CMOS performance trends," *IEEE Trans. Electron. Devices*, vol. 48, no. 8, pp. 1776–1782, Aug. 2001.
- [6] J.-P. Colinge et al., "Nanowire transistors without junctions," *Nature Nanotechnol.*, vol. 5, no. 3, pp. 225–229, 2010.
- [7] S. Kanungo, S. Chattopadhyay, P. S. Gupta, and H. Rahaman, "Comparative performance analysis of the dielectrically modulated full-gate and short-gate tunnel FET-based biosensors," *IEEE Trans. Electron. Devices*, vol. 62, no. 3, pp. 994–1001, Mar. 2015.
- [8] M. Kumar, M. A. Hussain, and S. K. Paul, "Performance of a two input nand gate using subthreshold leakage control techniques," *J. Electron. Devices*, vol. 14, pp. 1161–1169, Jun. 2012.
- [9] M. J. Kumar and K. Nadda, "Bipolar charge-plasma transistor: A novel three terminal device," *IEEE Trans. Electron. Devices*, vol. 59, no. 4, pp. 962–967, Apr. 2012.
- [10] M. J. Kumar and S. Janardhanan, "Doping-less tunnel field effect transistor: Design and investigation," *IEEE Trans. Electron. Devices*, vol. 60, no. 10, pp. 3285–3290, Oct. 2013.
- [11] A. M. Ionescu and H. Riel, "Tunnel field effect transistors as energy efficient electronics switches," *Nature*, vol. 479, no. 7373, pp. 329–337, Nov. 2011.
- [12] K. Na and Y. Kim, "Silicon complementary metal-oxide-semiconductor field-effect transistors with dual workfunction gate," *Japanese J. Appl. Phys.*, vol. 45, no. 12, pp. 9033–9036, Dec. 2006.
- [13] W. Y. Choi, B.-G. Park, J. D. Lee, and T.-J. K. Liu, "Tunneling field-effect transistor (TFETs) with subthreshold swing (SS) less than 60 mV/dec," *IEEE Electron. Device Lett.*, vol. 28, no. 8, pp. 743–745, Aug. 2007.
- [14] B. Ghosh and M. W. Akram, "Junctionless tunnel field effect transistor," *IEEE Electron. Device Lett.*, vol. 34, no. 5, pp. 584–586, May 2013.
- [15] K. K. Bhuwalka, J. Schulze, and I. Eisele, "Scaling the vertical tunnel FET with tunnel bandgap modulation and gate workfunction engineering," *IEEE Trans. Electron. Devices*, vol. 52, no. 5, pp. 909–917, May 2005.
- [16] S. Tirkey, D. Sharma, B. Ram, and D. S. Yadav, "Introduction of a metal strip in oxide region of junctionless tunnel field-effect transistor to improve DC and RF performance," *J. Comput. Electron.*, vol. 16, no. 3, pp. 714–720, Sep. 2017.
- [17] C. Sahu and J. Singh, "Charge-plasma based process variation immune junctionless transistor," *IEEE Electron. Device Lett.*, vol. 35, no. 3, pp. 411–413, Mar. 2014.

- [18] B. R. Raad, S. Tirkey, D. Sharma, and P. Kondekar, "A new design approach of dopingless tunnel FET for enhancement of device characteristics," *IEEE Trans. Electron. Devices*, vol. 64, no. 4, pp. 1830–1836, Apr. 2017.
- [19] P. Bergveld, "Development of an ion-sensitive solid-state device for neurophysiological measurements," *IEEE Trans. Biomed. Eng.*, vol. 17, no. 1, pp. 70–71, Jan. 1970.
- [20] S. Anand and R. K. Sarin, "An analysis on ambipolar reduction techniques for charge plasma based tunnel field effect transistors," *J. Nanoelectronics Optoelectron.*, vol. 11, no. 4, pp. 543–550, 2016.
- [21] P. N. Kondekar, K. Nigam, S. Pandey, and D. Sharma, "Design and analysis of polarity controlled electrically doped tunnel FET with bandgap engineering for analog/RF applications," *IEEE Trans. Electron. Devices*, vol. 64, no. 2, pp. 412–418, Feb. 2017.
- [22] K. Boucart and A. M. Ionescu, "Double-gate tunnel FET with high-\$\kappa\$ gate dielectric," *IEEE Trans. Electron. Devices*, vol. 54, no. 7, pp. 1725–1733, Jul. 2007.
- [23] A. Gnudi, S. Reggiani, E. Gnani, and G. Baccarani, "Analysis of threshold voltage variability due to random dopant fluctuations in junctionless FETs," *IEEE Electron. Device Lett.*, vol. 33, no. 3, pp. 336–338, Mar. 2012.
- [24] D. Sarkar and K. Banerjee, "Fundamental limitations of conventional FET biosensors: Quantum-mechanical-tunneling to the rescue," in *Proc. Device Research Conf.*, 2012, pp. 83–84.
- [25] A. M. Ionescu and H. Riel, "Tunnel field-effect transistors as energy-efficient electronic switches," *Nature*, vol. 479, no. 7373, pp. 329–337, Nov. 2010.
- [26] S. Sahoo, S. Dash, and G. P. Mishra, "Work-function modulated hetero gate charge plasma TFET to enhance the device performance," in *Proc. Devices Integr. Circuit*, 2019, pp. 461–464.
- [27] H. Wang, S. Chang, J. He, Q. Huang, and F. Liu, "The dual effects of gate dielectric constant in tunnel FETs," *IEEE J. Electron. Develop. Soc.*, vol. 4, pp. 445–450, Nov. 2016.
- [28] H. Im, X.-J. Huang, B. Gu, and Y.-K. Choi, "A dielectric-modulated field-effect transistor for biosensing," *Nature Nanotechnol.*, vol. 2, no. 7, pp. 430–434, 2007.
- [29] N. Mustakim, S. Hussain, and J. K. Saha, "Characterization of charge plasma-based junctionless tunneling field effect transistor (JL-TFET)," in *Proc. IEEE Int. Symp. Smart Electron. Syst. (Formerly iNiS)*, 2020, pp. 40–43.
- [30] S. Yadav, D. Sharma, M. Aslam, and D. Soni, "A novel analysis to reduce leakage current in charge plasma based TFET," in *Proc. 14th IEEE India Council Int. Conf.*, 2017, pp. 1–3.
- [31] T. K. Bhardwaj, D. Kakkar, and B. Raj, "Comparative study of on-drive-current improvement techniques in charge plasma TFET," in *Proc. 3rd Int. Conf. Electron., Commun. Aerosp. Technol.*, 2019, pp. 122–127.
- [32] F. Jazaeri and J.-M. Salles, *Modeling Nanowire and Double-Gate Junctionless Field-Effect Transistors*. Cambridge, U.K., MA, USA: Cambridge Univ. Press, 2018.
- [33] W. Long, H. Ou, J.-M. Kuo, and K. K. Chin, "Dual-material gate (DMG) field effect transistor," *IEEE Trans. Electron. Devices*, vol. 46, no. 5, pp. 865–870, May 1999.
- [34] R. N. Ajay, M. Saxena, and M. Gupta, "Modeling and simulation investigation of sensitivity of symmetric split gate junctionless FET for biosensing application," *IEEE Sensors J.*, vol. 17, no. 15, pp. 4853–4861, Aug. 2017.
- [35] *ATLAS Device Simulation Software*. Santa Clara, CA, USA: Silvaco Int., 2014.
- [36] A. Densmore et al., "Spiral-path high-sensitivity silicon photonic wire molecular sensor with temperature-independent response," *Opt. Lett.*, vol. 33, no. 6, pp. 596–598, 2008.
- [37] D. Sarkar and K. Banerjee, "Proposal for tunnel-field-effect-transistor as ultra-sensitive and label-free biosensors," *Appl. Phys. Lett.*, vol. 100, no. 14, 2012, Art. no. 143108.
- [38] G. Wadhwa and B. Raj, "Parametric variation analysis of symmetric double gate charge plasma JLTFET for biosensor application," *IEEE Sensors J.*, vol. 18, no. 15, pp. 6070–6077, Aug. 2018.
- [39] J. Madan, R. Pandey, R. Sharma, and R. Chaujar, "Impact of metal silicide source electrode on polarity gate induced source in junctionless TFET," *Appl. Phys. A*, vol. 125, no. 9, pp. 1–7, 2019.
- [40] J. Madan, M. Dassi, R. Pandey, R. Chaujar, and R. Sharma, "Numerical analysis of Mg2Si/Si heterojunction DG-TFET for low power/high performance applications: Impact of non-idealities," *Superlattices Microstruct.*, vol. 139, 2020, Art. no. 106397.